Title

Effect of subsurface soil moisture variability and atmospheric conditions on methane gas migration in shallow subsurface

Authors

Deepagoda, TKK Chamindu
Smits, Kathleen M
Oldenburg, Curtis M

Publication Date

2016-12-01

DOI

10.1016/j.ijggc.2016.10.016

Peer reviewed

Effect of subsurface soil moisture variability and atmospheric conditions on methane gas migration in shallow subsurface

Chamindu Deepagoda T.K.K. [b], Kathleen M. Smits[a,*], Curtis M. Oldenburg[c]

[a] Center for Experimental Study of Subsurface Environmental Processes (CESEP), Department of Civil and Environmental Engineering, Colorado School of Mines, Golden, CO 80401, USA
[b] Department of Civil Engineering, University of Peradeniya, Peradeniya 20400, Sri Lanka

[c] Energy Geosciences Division, Lawrence Berkeley National Laboratory, 1 Cyclotron Road Berkeley, CA 94720, USA

a r t i c l e i n f o

Article history:
Received 1 June 2016
Received in revised form 21 October 2016 Accepted 28 October 2016
Available online 14 November 2016

Keywords:
Methane gas migration Natural gas Unsaturated soil
Gas transport Shallow subsurface

a b s t r a c t

A major concern resulting from the increased use and production of natural gas has been how to miti- gate fugitive greenhouse gas emissions (predominantly methane) from natural gas infrastructure (e.g., leaky shallow pipelines). Subsurface migration and atmospheric loading of methane from pipeline leak- age is controlled by source configurations and subsurface soil conditions (e.g., soil heterogeneity and soil moisture) and are further affected by atmospheric conditions (e.g., wind and temperature). How- ever, the transport and attenuation of methane under varying subsurface and atmospheric conditions are poorly understood, making it difficult to estimate leakage fluxes from methane concentration mea- surements at and above the soil surface. Based on a series of controlled bench-scale experiments using a large porous media tank interfaced with an open-return wind tunnel, this study investigated multiphase processes controlling migration of methane from a point source representing a buried pipeline leaking at fixed flow rate (kg/s) under various saturation and soil-texture conditions. In addition, potential effects of atmospheric boundary controls, wind (0.5 and 2.0 m s^{-1}) and temperature (22 and 35 °C), were also examined. Results showed the distinct effects of soil heterogeneity and, to a varying degree, of soil mois- ture on surface methane concentrations. In addition, results also showed the pronounced effects of wind and, to a lesser degree, of temperature on surface methane concentrations in the presence of varying soil and moisture conditions. The observed subsurface methane profiles were simulated using the mul- tiphase transport simulator TOUGH2-EOS7CA. Observed agreement between measured and simulated data demonstrates that for the conditions studied, multiphase migration of a multicomponent gas mix- ture (including methane) under density-dependent flow can be adequately represented with a Fickian advection-diffusion (or dispersion) model (ADM) framework. The dominant effect of saturation over the soil texture, could also be inferred from numerical characterization.

1. Introduction

Despite continuing efforts to reduce greenhouse gas loading to the atmosphere to mitigate climate change, anthropogenic emis- sion of greenhouse gases has accelerated during the last decade (2000–2010) compared to the preceding decade (Intergovernmen- tal Panel for Climate Change; IPCC, 2014). The energy supply sector (inclusive of all energy extraction, conversion, storage, and trans- mission to final-users), the largest contributor to global greenhouse gas emissions, was responsible for 35% of the total anthropogenic emissions in 2010 (IPCC, 2014). Consequently, the energy sector has recently received renewed attention with the perspective of reducing future emissions by adopting low-carbon technologies in energy production. Fossil fuel-switching, in particular, is consid- ered a promising strategy to reduce greenhouse gas emissions from the electricity-generation sector. Natural gas, in this regard, plays a role as a "transition fuel" when shifting from the high-carbon fossil fuels (coal and oil) to more environmentally-friendly renew- able energy substitutes in the future (Levi, 2013). Notably, natural gas has a considerably smaller greenhouse gas footprint compared to that of coal in terms of greenhouse gas emissions per unit of energy produced in fossil fuel chains; natural gas is less intensive (290–930 gCO_2eq/kWh) than oil (510–1170 gCO_2eq/kWh) and coal

* Corresponding author at: Center for Experimental Study of Subsurface Envi- ronmental Processes (CESEP), Department of Civil and Environmental Engineering, Colorado School of Mines, Golden, CO, 80401, USA.
E-mail address: chamindu78@yahoo.com (T.K.K. Chamindu Deepagoda).

http://dx.doi.org/10.1016/j.ijggc.2016.10.016
1750-5836/

Nomenclature

D_{κ}	Molecular diffusivity of component K in phase ϕ ($m^2\ s^{-1}$)
g	Gravitational acceleration vector (m s^{-2})
F	Darcy flux vector (kg $m^2\ s^{-1}$)
k	Intrinsic permeability (m^2)
k_{r}	Relative permeability (−)
M	Mass accumulation term (kg m^{-3})
n	Outward unit normal vector
P	Total pressure (Pa)
P_c	Capillary pressure (Pa)
q	Mass flux (kg $m^{-2}\ s^{-1}$)
S	Saturation (−)
S_{β}	Saturation (−)
t	Time (s)
T	Temperature (°C)
u	Wind velocity (m s^{-1})
V	Volume (m^3)
X_{κ}^{β}	Mass fraction with phase subscript and component superscript (−)
X Y Z	X-coordinate (m) Y-coordinate (m) Z-coordinate (positive upward) (m)
TD	Exponent for temperature dependence of diffusivity (−)

Greek symbols

α	1/Po in van Genuchten's capillary pressure function (Pa^{-1})
β	Phase index (subscript)Phase index (subscript) Surface area (m^2)
ϕ	Mass components (superscript)
μ	Dynamic viscosity (kg $m^{-1}\ s^{-1}$)
ρ	Density (kg m^{-3})Density (kg m^{-3})
τ	Tortuosity (−)
φ	Porosity ($m^3\ m^{-3}$)

Subscripts and superscripts

g	Gas
l	Liquid
w	Water
S	Saturation
max	Maximum
r	Residual
0	Reference value

(675–1689 gCO_2eq/kWh) (IPCC, 2011) and therefore is a promising energy surrogate for the coming decades (Cathles et al., 2012).

However, fugitive atmospheric emissions from leaky natural gas infrastructure may largely offset intended environmental benefits of natural gas usage since methane (CH_4), the predominant com- ponent of natural gas, has a global warming potential 86 times greater than CO_2 on a 20-year basis and 25 times greater over a 100-year time horizon (Jackson et al., 2013). (Note that the greenhouse gas potency is sensitive to the time frame of interest because CH_4 is converted to CO_2 in decadal scales.) Recent stud- ies revealed that coal-to-gas switching would bring meaningful climate forcing benefits (in both short-term and long-term scenar- ios) provided fugitive CH_4 emissions are maintained below about 3% of gas production (Lelieveld et al., 2005). Nevertheless, the lat- est statistics on atmospheric methane leaks in gas supply chains are not conclusive and vary between 5%–1% (e.g. Howarth et al., 2011; Cathles et al., 2012). The present inventory-based leakage estimates are particularly incomplete and involve a wide range of uncertainties including invalidated emission factors (Karion et al., 2013; Lamb et al., 2015), undercounted "super-emitters" (Brandt et al., 2014), underrepresented high-emission production tech- nologies (e.g., liquid unloading; API/ANGA, 2012), and unsolved issues in emission estimation methods (e.g., Pétron et al., 2012; Levi, 2012), etc. Several pipeline emission surveys conducted along major U.S. urban city roads also revealed surprisingly high CH_4 leaks (Jackson et al., 2013; Phillips et al., 2013) which were gener- ally attributed to the aging underground gas infrastructure (USEPA, 2014) where more recently, Lamb et al. (2015) reported decreas- ing methane emissions. Importantly, all estimates, predictions, and recommendations in the USEPA (2014) study were made based on above-ground concentration measurements, with very limited attention paid to the controlling mechanisms of fate and transport of natural gas/methane in the shallow subsurface around the leak- ing pipelines under differing near-surface atmospheric controls.

Natural gas gathering, transmission and distribution pipelines range in material composition from high strength steel or copper to flexible plastic and can range in size from 40 to 6 in. in diameter, depending on the location and use (Folga, 2007; Transportation of Natural Gas, 2016). Although new steel and plastic pipelines are less prone to leaks than their older counterparts, aged pipelines, made

of cast iron or unprotected steel, often leak due to earth move- ment, breakdown of joints and corrosion of unprotected steel, and graphitization (i.e., natural degrading to softer elements over time) of iron pipelines. Pipelines are usually placed in a trench 1.5–4 feet below ground. In the U.S., the depth is specified according to fed- eral regulations (Transportation of Natural Gas, 2016) and depends on the pipe diameter, soil or rock type, terrain characteristics, etc. Upon laying the pipe, the trench is backfilled with excavated mate- rial. As backfilling often involves mechanical compaction (causing a low-permeability zone), additional materials, sometimes of differ- ent soil types, are used to achieve a level surface. If the excavation was done in rocky formations, a layer of broken rocks may be placed above the pipeline thus forming a high-permeability layer. In brief, differently- characterized layers are often found within the back- fill zone above a leaky pipeline, which may markedly affect the subsurface methane migration.

Transmission mains typically carry natural gas at high-pressure conditions (3500–9600 kPa) whereas low pressure conditions (1.5–2000 kPa) prevail in distribution systems. Consequently, in the event of a leak, the mechanism of gas emission into the sur- rounding porous medium, as well as the domain of influence of the leak, will vary depending upon the pressure conditions of the pipelines. In practice, high-pressure (advection-controlled) leaks are relatively easy to detect and fix up, while detecting small and diffusion-controlled leaks, as is the case presented in this study, is challenging.

The methane migration length scales from a leaky distribution pipeline may vary broadly in the range of 2–10 m (Okamoto and Gomi, 2011, Yan et al., 2015, and Xie et al., 2015) depending upon the burial depth, soil properties and moisture status (discussed below) as well as on the gas composition. With regard to gas compo- sition, natural gas is composed almost entirely of methane (>94%) in transmission and distribution systems, however less methane con- tents may present in production (79%) and processing (87%) stages. (USEPA, 2003).

Fate and transport of methane in soil are primarily controlled by subsurface conditions such as heterogeneity, soil moisture, temper- ature, and pressure gradients (Poulsen et al., 2003). For example, gas migration in a texturally heterogeneous soil system (e.g., in the presence of a low-permeability clay lens embedded in a sandy formation) will be markedly different from that of a homogenous soil system due to the different texture- (or porosity-) induced tortuosity effects (Ho and Webb, 2006). Similarly, soil moisture

controls methane migration in variably-saturated soils because of attenuation due to methane solubility, oxidation, and water- induced tortuosity (Smith et al., 2003) and simultaneous water vapor transport in the soil gas phase. Furthermore, temperature affects molecular diffusion and thereby the diffusive flow of gases while the presence of pressure gradients leads to advective gas flow. Methane flow regimes are typically dominated by advective flow near the leak (due to high pipeline pressure) and become diffusion-controlled as gas migrates away from the point of leak- age. Moreover, the wind- or temperature-induced near-surface fluctuations may also affect the subsurface migration and atmo- spheric emission of methane (Poulsen et al., 2003). However, to our knowledge, only a limited number of combined experimental and numerical studies investigating subsurface methane migration under different subsurface conditions and atmospheric controls have been reported in literature.

Previous laboratory-based studies investigating methane (or other natural gas-related gases; e.g., CO_2, propane) migration in soil/porous media mainly involved one-dimensional column experiments (Hibi et al., 2009, 2012; Karl-Heinz et al., 2004). In most studies, a single- or multi-component gas (or a gas mixture) was applied through a uniformly packed soil column under a con- stant flow rate (or a pressure gradient) and gas concentrations were measured at selected ports along the column. A few field- scale two- or three-dimensional natural gas transport studies have also been performed to investigate gas (CH_4 or CO_2) concentration profiles across differently-characterized soil profiles (e.g., Okamoto and Gomi, 2011; Yan et al., 2015), however, literature on the effect of the degree of saturation on methane concentration profiles could not be found.

Experimental gas transport studies in coupled domains of porous media and free flow are particularly rare in the literature. Based on a recent two-dimensional study in a sand-packed tank interfaced with a free flow (atmospheric) domain, Basirat et al. (2015) investigated CO_2 migration from a buried point source in both porous media and free flow domains, but did not consider the effects of any atmospheric controls on surface-subsurface gas trans- port processes. The experimental results, in general, commonly identified the effect of gas density on gas flow characteristics; high- density gases (e.g., CO_2, propane) were found to migrate downward and accumulate in the zone below the gas source while low-density gases (e.g., CH_4, H_2) preferentially moved upward by buoyancy. Further, laboratory-based experimental studies on heterogeneous and variably saturated porous media distinguished differences in gas-transport behavior of different zones e.g., the preferential flow regions or low-permeability zones (Volckaert et al., 1995; Delahaye and Alonso, 2002; Okamoto et al., 2014) in relation to advective and diffusive gas migration.

Most numerical approaches presented in the literature on mod- eling the migration of multicomponent gas mixtures in porous media are primarily founded on the classical advection-diffusion (or dispersion) model (ADM), which combines Darcy's law (advec- tion) and Fick's law (ordinary diffusion) (Abriola and Pinder, 1985a,b; Slough et al., 1999; Okamoto and Gomi, 2011). The mod- els varied widely depending on whether they consider or ignore the effects of gas density, non-isothermal flow properties, real-gas mixture properties (e.g., temperature dependence on gas den- sity, viscosity, and solubility), compressibility etc. A wide range of studies using the concept of the Dusty Gas Model (DGM) (Cunningham and Williams, 1980; Mason and Malinauskas, 1983) for simulating multicomponent gas flow can also be found in the literature (e.g., Webb, 1998; Hibi et al., 2009). The applicability of the DGM concept was found to be essentially important in low-
permeability formations (e.g., graphite $k \sim 10^{-18}\,m^2$; Webb, 1996)
where molecular-wall interactions and thus Knudsen diffusion plays an important role in diffusive mass transport. However, for

high-permeability porous media ($k > 10^{-15}\,m^2$), as is the case in the present study, the results from AD and DG models were observed to be comparable (Oldenburg et al., 2004; Hibi et al., 2009), and a good agreement was often observed between AD-modelled and measured data (e.g., Okamoto and Gomi, 2011). Nevertheless, the applicability of the Fickian diffusion approach for multicomponent gas transport modeling needs to be further verified with experi- mental observations. In addition, limited numerical studies were found for simulating CH_4 (or CO_2) migration in coupled porous media and atmospheric domains (e.g., Oldenburg and Unger, 2004; Basirat et al., 2015) which also motivates validation with experi- mental observations.

Based on a controlled bench-scale experimental and numerical study, we investigated methane (mixed with air and water vapor) migration under carefully controlled subsurface and atmospheric conditions. The key hypotheses of this study are: (i) the subsurface migration of multicomponent gas mixtures and the development of the atmospheric concentration boundary layer are essentially con- trolled by subsurface conditions (e.g., soil moisture, heterogeneity) and atmospheric controls (near-surface wind and temperature); (ii) the degree to which the controlling parameters (described in hypothesis (i)) affect the subsurface methane flow and transport can be experimentally evaluated in a coupled two-dimensional porous media-wind tunnel test facility at a bench-scale; and (iii) experimentally identified effects (described in hypothesis (ii)) can be numerically simulated by modeling density-dependent flow of a multicomponent real-gas mixture (CH_4, air and water vapor) by the Fickian ADM under constrained atmosphere boundary condi- tions. We emphasize that the results are based on the length scales of the experimental and numerical domains which may not truly mimic more realistic soil-atmosphere continuum scales at specific pipeline-soil systems.

2. Materials and methods

2.1. Experimental set-up and porous media

A series of controlled bench-scale laboratory experiments was conducted using a low-velocity open-return wind tunnel inter- faced with a 2D soil tank of dimensions 35 cm 55 cm 10 cm (height length width) as illustrated schematically in Fig. 1.

The ductwork forming the wind tunnel was aligned with the tank to channel heated air flow across the test section. To create and control the wind velocity, the wind tunnel was equipped with an in-line duct fan (Fasncourt Pro Model DB6GTP, 15.2 cm diameter) connected with a variable velocity controller, and a gal- vanized 15-cm circular damper (Davarzani et al., 2014). The wind velocity was continuously measured by means of a pre-calibrated pitot static tube (Dwyer Instruments, Inc. Model 167-12, 0.32 cm diameter, 30.48 cm insertion length, accuracy 65%) connected to a differential pressure transmitter (Omega Engineering, Inc.
Model PX653-0.1D5V, Range 50–0.1 in. of H_2O, 0–25 Pa). For high- temperature (35–40 °C) measurements, a constant heat pulse was applied by means of an infrared heater located upstream (80 cm from the test section) of the wind tunnel. The heater assembly con- sisting of five infrared heater units (Mor Electric Heating Assoc., Inc. Infrared Salamander Model FTE 500-240) was placed in parallel within a reflector. The heater and the fan were operated a minimum of 3 h ahead of the experiment to allow sufficient time to reach steady state in terms of air and heat flow by the onset of the exper- iment. Temperature/relative humidity sensors (Decagon Devices Inc.

EHT RH/Temperature, accuracy 62% from 5 to 90% RH, 63% from 90 to 100% RH, temperature accuracy 0.25 $^{\circ}$C) were placed immediate upstream and downstream of the test section at two levels above the surface: 0 cm (i.e., at the surface) and 17 cm. Methane

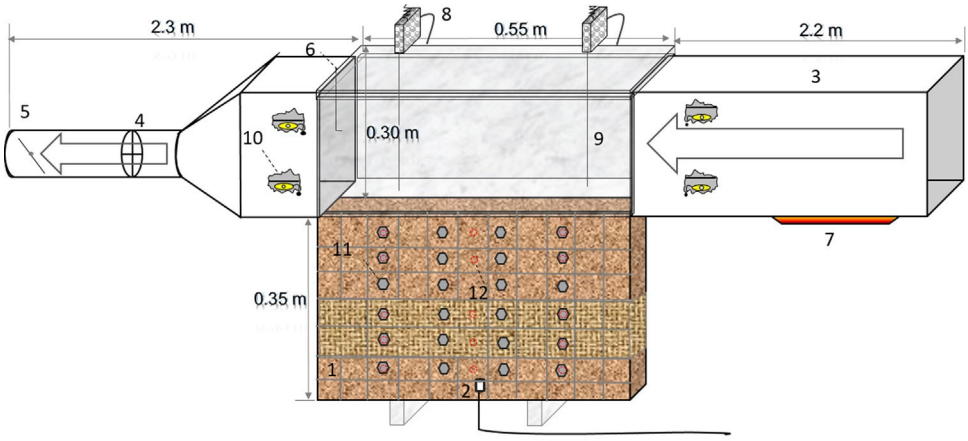

Fig. 1. Schematic of the experimental set-up (not to scale). The arrows show the wind direction. The symbols (&) denote sensor locations for soil moisture (in the front side) and temperature (in the back side), respectively.

concentrations within the wind tunnel test section were measured using an atmospheric fast flame ionization detector (fast FID) sys- tem (HFR 400, Cambustion Ltd, UK, relative sensitivity to methane, 0.97). The sampling head assembly (2 Nos.) was mounted on a laterally movable frame to facilitate length-wise measurements (i.e., along the soil surface). Provisions were also made for vertical movements to measure methane concentrations from 0 to 18 cm above the soil surface. A 20-cm long capillary tube was attached to each sampling head to extract methane gas (50 cm^3/min) at a pre- set pressure gradient of 150 mm Hg (response time = 1–2 ms). The operating combustion temperature at steady state was maintained at 250–300 °C (per manufacturer's recommendation) and remained constant throughout the experiments. Prior to each experiment, a calibration test was conducted (at the above temperature) using five standard methane gas concentrations (in ppm): 10, 100, 1000, 10000, and 50000. A strong linear relation ($r^2 > 0.98$) between the concentration (ppm) and the response signal (mV) was observed in all cases. In addition, background methane concentrations were monitored and considered in the measurements/calculations (on average 2 ppm). All above-surface measurements including wind velocity, temperature, relative humidity, and methane concen- tration were monitored continuously, real-time, using LabVIEW software (National Instruments Corp.).

An integrated sensor network embedded into the soil tank was used to measure soil temperature (15 Nos, Decagon Devices Inc. RT-1, accuracy ±0.5 °C from 5 to 40 °C) and moisture (24 Nos, Decagon Devices, Inc. ECH$_2$O EC-5, measurement frequency 570 MHz, accu- racy 63%). The soil moisture sensors were individually calibrated before measurements following Sakaki et al. (2008). A point gas source (50,000 ppm CH_4 and 950,000 ppm N_2, flow rate = 0.5 lpm) was placed 2 cm above the bottom of the tank (at the centerline) to mimic a diffusion-dominant leak from a shallow underground pipe. Note that the selected flow rate (0.5 lpm) is within the rage of field-estimated leakage rates (0.002–12.9 lpm) from distribution systems reported in the literature (e.g. GRI/EPA, 1996; GTI, 2013; EPA, 2014; Lamb et al., 2015) No noticeable temperature change was recorded in the vicinity of the gas source at the onset of injec- tion and the ambient temperature conditions, as controlled by the surface temperature, prevailed near the source.

The tank was packed uniformly with a silica sand # 30/40 (identified by the effective sieve number) (Accusand, Unimin Cor- poration, Ottawa, MN) to represent a homogenous system. To represent a layered system, a 5-cm thick coarse-textured (#12/20) sand layer was sandwiched 15 cm below the surface. The layered test configuration was selected based on its simplicity (simple soil heterogeneity) and the locations of the soil moisture sensors and sampling ports (discussed below). Also, the location of the coarse-textured layer allows for the development of variable soil water saturation based on the soil's hydraulic properties (discussed below).

Experiments were conducted for near-dry (i.e., at residual saturation) and partially saturated (i.e., wet-packed and drained to 35 cm H_2O with respect to the center of the tank) conditions. Basic thermo-physical properties of the two porous media are given in Table 1, which also presents van Genuchten parameters used for numerical simulations. The high chemical purity and the presence of only a trace amount of organic carbon (0.03%) is a notable feature of both sand types, which limited the potential for methane oxida- tion due to microbiological functions during the experiments. For further details on the two sand types, measurement methods and packing conditions, see Smits et al. (2012).

To confirm that steady-state conditions were achieved prior to the start of the experiments, surface methane concentrations were continuously monitored at two selected locations on the soil surface until the time-invariant concentrations were recorded for 1–2 h using the Fast FID system. At steady state, gas samples (1 ml) were extracted (in triplicates) from selected ports at depths (mea- sured from the surface) of 0.5, 7.5, 17,5, 30 cm using a high-precision analytical syringe (VICI Precision Sampling, Inc., LA) and methane concentrations were measured (with no time lag) using gas chromatography (Agilent Technology, 6890). The sam- pling ports are located vertically along the centerline of the tank and at the rear side of the tank (not shown in Fig. 1).

In total, 24 experiments were conducted (Table 2): 2 soil states (homogenous and layered) × 2 [illegible] and partially-saturated) × 3 wind velocities (0, 0.5, 2.0 ms^{-1}) × 2 atmospheric temperatures (22 °C and 35 °C). Experiments were selected to test the control of subsurface conditions (e.g. soil moisture, hetero- geneity) and atmospheric controls (wind and tempertature) on

Table 1
Physical properties and transport parameters of the two porous media.

Porous media #	Particle diameter (D50)	Particle density (ρ_d)	Total porosity ($<I$)	Bulk density (ρ_b)	Saturated hydraulic conductivity (Ksat)	Thermal conductivity ( )		Gas Diffusivity[a] Ds/Do	Van Genuchten parameters[b]			Permeability	
	mm	g cm−3	cm3 cm−3	g cm−3	cm s−1	Wm−1 K−1			0_r (cm3 cm−3)	a (cm^{-1})	n (−)	kc (m2)	
12/20	1.04	2.665	0.33	1.82	0.376	0.314	2.948	0.201	0.056	0.053	13.5	3.8×10^{-10}	
30/40	0.53	2.665	0.336	1.77	0.106	0.287	2.887	0.184	0.017	0.1	9.21	1.0×10^{-10}	

[a] Measured independently using one-chamber diffusion apparatus (Taylor, 1949), see Chamindu Deepagoda et al. (2016).
[b] $m = 1–1/n$.
[c] Estimated from K_{sat} assuming fluidity of 9.81 × 106 m−1 s−1 at 20 ◦C.

Table 2
Experimental schedule and the notations used to describe different experimental conditions.

			Above Ground Controls					
			Low Temp. (20–24 °C)			High Temp. (35–38 °C)		
			u = 0 ms^{-1}	u = 0.5 ms^{-1}	u = 2.0 ms^{-1}	u = 0 ms^{-1}	u = 0.5 ms^{-1}	u = 2.0 ms^{-1}
Below Ground Controls	Near dry	Homogeneous	ND-HG-LT			ND-HG-HT		
		Layered	ND-LY-LT			ND-LY-HT		
	Partially-sat	Homogenous	PS-HG-LT			PS-HG-HT		
		Layered	PS-LY-LT			PS-LY-HT		

ND, Near-dry; PS, Partially-saturated; HG, Homogenous; LY, Layered; LT, Low temperature; HT, High temperature

the subsurface migration of methane gas. Three experiments were duplicated (not shown in Table 2) to confirm the repeatability of the measurements. In the following text, we follow the notations in Table 2 (presenting saturation-soil state-temperature combina- tions) to describe results relevant to the different scenarios.

All the experiments were conducted within a barometrically closed building under invariant barometric pressure conditions. The experimental set up was located within the laboratory in such a way that the induced pressure gradients (e.g, due to opening/closing of doors) minimally influence the experimental results. The passersby were restricted within the experimental area during the experiments to avoid likely pressure fluctuations. Pressure sensors installed within the building were randomly checked to ensure constant pressure conditions.

Table 3
Governing equations pertinent to this study as solved in TOUGH2/EOS7CA. Description Equation

Mass and energy balance $\frac{d}{dt}\int_V M^K dV_n = \int_{\Gamma} \boldsymbol{F}^K \cdot n d\Gamma + \int_V q^K dV_n$

Mass accumulation $M^K = \phi \sum_\beta S_\beta \rho_\beta X^k_\beta$

Phase flux $\boldsymbol{F}_\beta = -k \frac{k_{r\beta}\rho_\beta}{\mu_\beta}(\nabla P_\beta - \rho_\beta g)$

Component flux: advective and diffusive

$\boldsymbol{F}^k = \boldsymbol{F}^{adv}_\beta + \boldsymbol{F}^{dif}_\beta$

$\boldsymbol{F}^{adv}_\beta = X^k_\beta \boldsymbol{F}_\beta$

$\boldsymbol{F}^{dif}_\beta = -\tau\phi S_\beta \rho_\beta D^k_\beta \nabla X^k_\beta; D^k_\beta(T) = D^k(T_o)\left(\frac{T}{273.15}\right)^{\theta}$

Relative permeability (van Genuchten, 1980)

T_D

$k_{rl} = \sqrt{S^*}\left\{1 - \left(1 - [S^*]^{1/A}\right)^A\right\}^2$ if $S < S_{ls}$

$)_A^{1}{}_2$

2.2. Numerical model

Numerical simulations were performed using the multiphase transport simulator TOUGH2 (Pruess et al., 1999) combined with the equation of state module EOS7CA (Oldenburg, 2015). TOUGH2/EOS7CA simulates the subsurface flow and transport of aqueous and gas phases containing five components (i.e., H_2O, brine, non-condensable gas (e.g., CH_4), gas tracer, and air) under

Capillary pressure (van Genuchten, 1980) Henry's law

if $S_l \geq S_{ls} k_{rl} = 1$ if $S_{gr} = 0 k_{rg} = 1 - k_{rl}$

$$\hat{S} = (S_l - S_{lr}) / (S_{ls} - S_{lr})$$

$$Pc = Po\ [S^*]^{-1/A} - 1 \quad -$$

subject to $- Pmax \leq Pc \leq 0$

$PK = KHXw$

$$2 \qquad) \qquad (\qquad)_1$$

$$A$$

$$g$$

isothermal or non-isothermal conditions. The model approxi- mates air as a mixture of 79% N_2 and 21% O_2 by volume. TOUGH2/EOS7CA uses thermodynamic properties in real gas mix- tures (i.e., density, enthalpy departure and viscosity) calculated using the Peng–Robinson equation of state model (Peng and Robinson, 1976). A temperature-dependent Fickian molecular dif- fusion coefficient is used to model gas diffusion. Henry's law models dissolution of gaseous methane in the aqueous phase, with Henry's coefficients estimated using the method presented by Cramer (1982). The Henry's law approach in the model is accurate for low pressure (less than approx. 1 MPa) conditions and hence the model is applicable to relatively shallow subsurface porous media sys- tems (Oldenburg, 2015) as considered in this study. The reader is referred to Pruess et al. (1999) and Oldenburg (2015) for the full model description; however, the governing equations relevant to the present study are given in Table 3.

The simulations were done using a 2-D Cartesian computa- tional domain discretized into 63 "porous" elements representing the porous (subsurface) system with an additional "atmospheric" element (characterized with unit total porosity, infinitely large volume, and high permeability) coupled with the surface porous elements to represent the wind tunnel region (atmosphere). To simulate gas flow in partially-saturated conditions, a pre- simulation (without gas flow) was first performed using measured saturation data from different depths. The pre-simulation allowed for the model to reach saturation-capillary pressure equilibrium at the steady state. This was followed by a complete steady-state sim- ulation using the pre-simulation data together with gas flow. Due

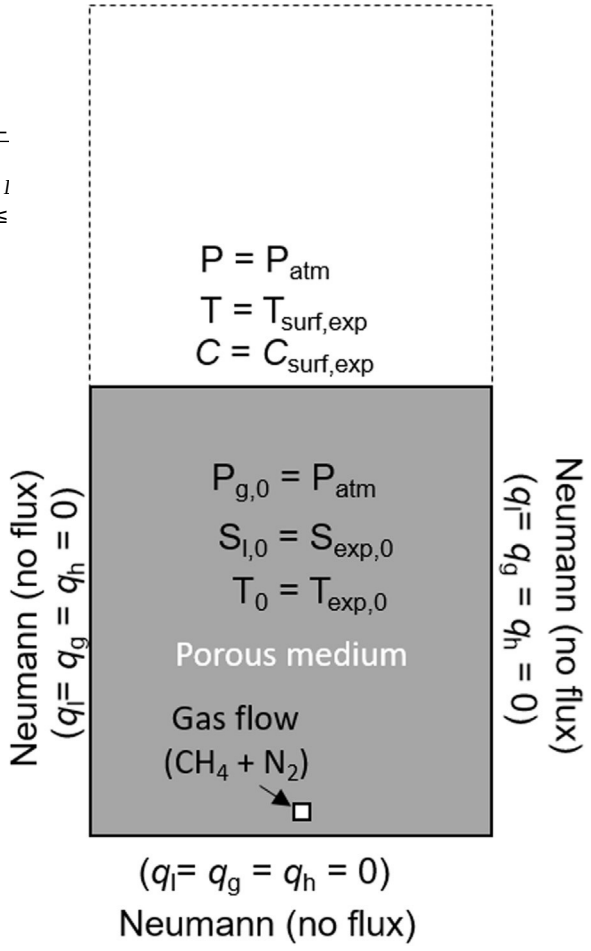

Fig. 2. Initial and boundary conditions used for the porous medium (subsurface) computational domain in TOUGH2/EOS7CA simulations. q_l denotes the liquid flux, q_g the gas flux, q_h the heat flux, respectively. The subscript *exp* denotes the exper- imental data. The dotted lines show the free flow domain. The source/inflow of CH4 and N2 gas mixture (CH4: 50,000 ppm, 2.9425E–07 kg/s; N2: 950,000 ppm, 1.0200E–05 kg/s) is also shown.

to the high purity of the two sands (Schroth et al., 1996), the bio- logical attenuation of methane could be reasonably neglected. The adopted initial and boundary conditions are shown in Fig. 2.

3. Results and discussion

3.1. Experimental results

3.1.1. Surface methane concentrations

The surface CH_4 concentrations measured ~0.5–1.0 mm above the surface) along the soil surface using the Fast FID method are shown in Fig. 3 for selected control conditions. Wind, in particular, showed a strong effect on surface CH_4 concentration variations as compared to the effect of temperature. In all cases, the no-wind condition (i.e., u = 0 ms^{-1}) showed the highest surface CH_4 concen- trations which decreased with increasing wind velocity. Notably, the observed surface CH_4 concentration profiles for the no-wind condition were mostly irregular with no mathematically express- ible pattern, except for a few profiles (e–h) showing near-constant concentrations along the surface. The observed irregular behavior could be attributed to the mixing and circulation of the differently dense air and methane within the test section. Nevertheless, the corresponding profiles for higher velocities (u = 0.5 and 2.0 ms^{-1}) could be adequately described with a simple nonlinear paramet- ric power function (Eq. (1)). Similar empirical power-law functions

$$C_s(x) = C_{s,o}$$

where L (cm) is the length of the tank, $C_{s,o}$ (ppm) is the maximum surface concentration (at the downstream edge), and n (−) is the shape factor representing the shape of the surface CH_4 concentra- tion buildup under different wind conditions. The fitted models are also illustrated in Fig. 3 in corresponding lines. Generally, for the wind velocities of 0.5 and 2.0 m s^{-1}, $C_{s,o}$ ranged between 2530 and 5150 ppm and 1190–2190 ppm, respectively, implying the wind- induced erosion of the surface methane concentration boundary layer. The n value, on the other hand, varied in the ranges of 0.2–0.3 and 0.5–0.65, respectively. Note that n = 0 in Eq. (1) mathematically represents the no-wind condition with a constant concentration (C-$C_{s,o}$) along the surface as also observed with some no-wind con- centration profiles (Fig. 3e–h). Further observations, however, are required to derive a statistically meaningful relationship between n and wind velocity (u).

The temperature generally increased the surface methane concentration but to varying degrees, as shown in Fig. 3. This is likely due to the changes in the thermodynamic proper- ties of methane at high temperature, causing decreased density and increased diffusivity and thermal conductivity, resulting in increased temperature-induced diffusive methane fluxes to the atmosphere. High temperature effects were expected at high-wind conditions due to the heated-up air passing over the soil surface, enhancing diffusive emissions. Indeed, at partially-saturated con- ditions, the heated air flow heats up the soil surface over time and tends to dry out the near-surface soils. This increases air-filled pore spaces and facilitates methane emissions. The temperature effects were more evident in no-wind conditions, although the results were somewhat obscured by the marked fluctuation in observed data (note that the error bars show one standard deviation from the mean value). Despite the expected higher temperature effects at high-wind conditions, the wind effects were dominant over the temperature effects in the methane concentration profiles. Note that the temperature-induced effects, to some extent, were evident also at $u = 0.5\ ms^{-1}$, however were largely masked at $u = 2.0\ ms^{-1}$ by the pronounced wind effects.

3.1.2. *Depth-wise variation of temperature and water saturation*

The depth-wise temperature variations are shown in Fig. 4 for all the subsurface and atmospheric conditions. In addition to experimental observation, the temperature profiles are needed to estimate the heat loss (which was very small) out of the plexiglass walls of the tank in the model. Note that the distinctly low temper- atures in Fig. 4(a) for low-temperature measurements were due to the low ambient air temperature at the time of the experiments. As expected, the temperature at the surface and in the topsoil (0 to –10 cm) was highest for high-air temperature, high-velocity conditions due to heated air movement along the soil surface. The temperature below 15 cm depth, however, remained mostly unaffected by above-surface temperature variations, though a slight subsurface 'cooling effect' could be seen at high surface tem- perature conditions particularly for partially-saturated soils due to the latent heat transfer for soil-water vaporization. Importantly, no effect due to the presence of the coarse-textured layer could be seen on temperature profiles presumably due to the similar thermal con- ductivity values for fine-textured (#30/40) and coarse-textured (# 12/20) media for both dry and partially-saturated conditions (see Table 1).

Fig. 5 shows the depth-wise variation of water saturation under partially-saturated conditions for (a) homogenous and (b) layered soil systems. In contrast to the monotonically increasing saturation

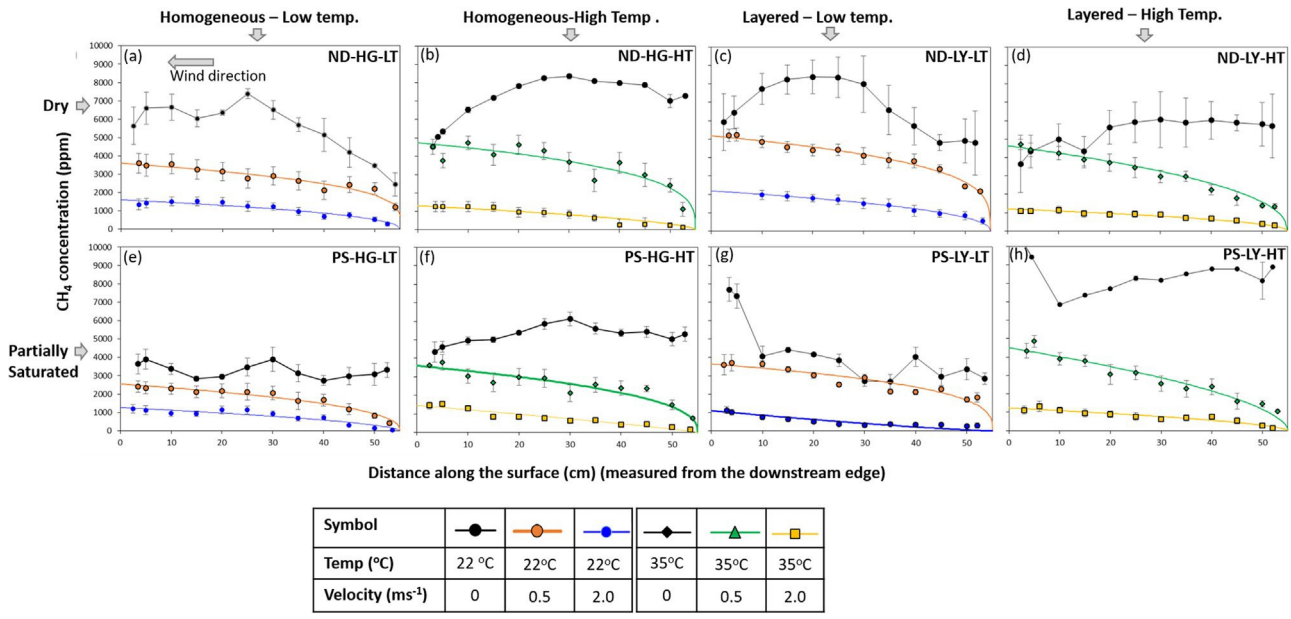

Fig. 3. Measured surface methane concentration (in ppm) as a function of the distance (in cm) along the surface (measured from the downstream edge of the test section) for 24 experimental conditions. Measurements for three wind velocities (0, 0.5, 2.0 ms^{-1}) are shown in corresponding colors in each sub-figure. The arrow (in 3a) shows the wind direction. The solid lines (in corresponding colors) for 0.2 ms^{-1} and 0.5 ms^{-1} show the parameterized model (Eq. (1)) descriptions while the lines for 0 ms^{-1} show point-to-point linear interpolation. Error bars denote one standard deviation (±) from the average concentration ($n \geq 20$).

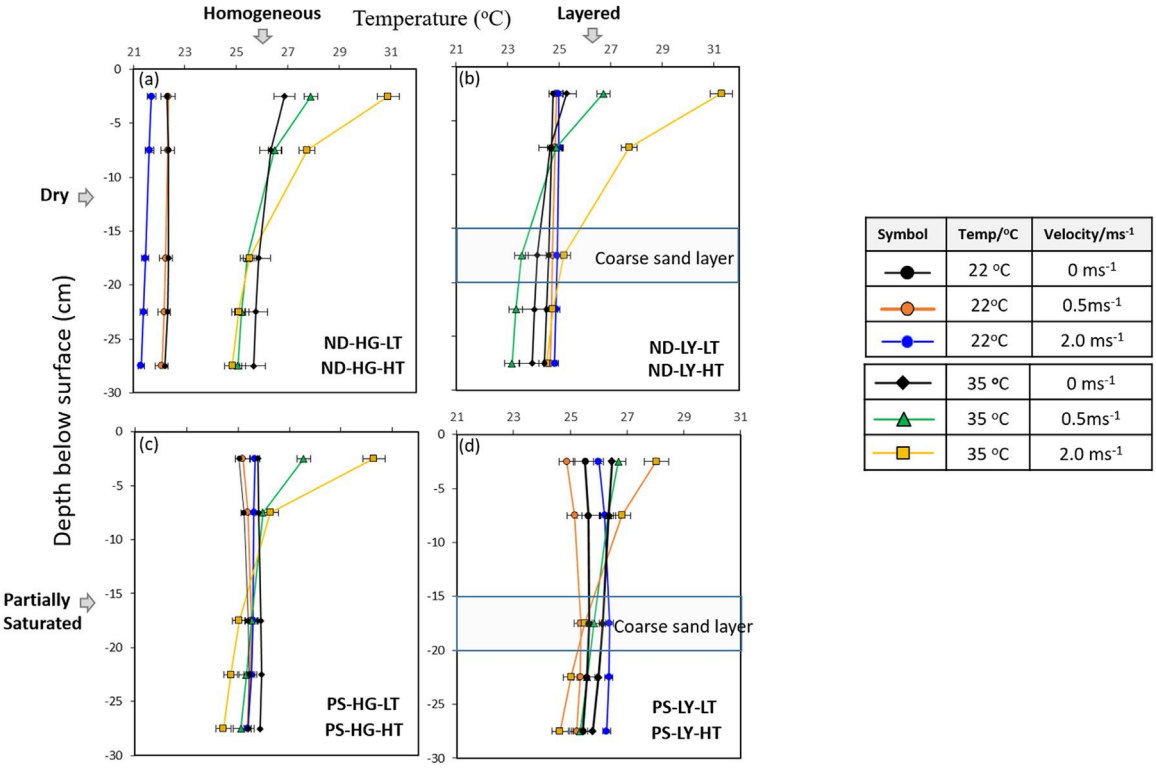

Fig. 4. Depth-wise variation of soil temperature (°C) for the 24 experimental conditions. Error bars denote one standard deviation (±) from the mean value ($n \geq 20$). The coarse-textured layer in the layered systems (4b and c) is demarcated by the two horizontal lines.

with depth in homogenous systems, the layered systems showed a distinct high-saturation (20%) region within the capillary barrier (approx. 2.5-cm above the textural interface; shown by the dotted line in Fig. 4b) and was underlain by the course-textured layer with relatively low saturation under steady state conditions. The capil- lary barrier effect is due to capillary tension that limits the water's downward movement from a finer soil into a coarser soil. A coarser

soil layer underlying a finer soil layer causes temporary water stor- age in the upper (finer) soil layer that can ultimately be removed by evaporation, lateral drainage or percolation into the lower layer (Stormont and Anderson, 1999). In fact, the steady state condi- tion with respect to saturation could not be ideally maintained under partially-saturated conditions as the surface evaporation, moisture movement and redistribution continuously evolved (at

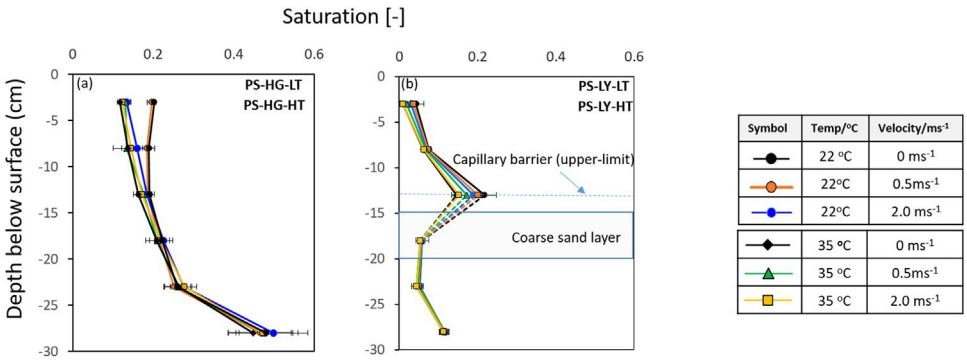

Fig. 5. Depth-wise variation of saturation for the partially-saturated (a) homogenous and (b) layered systems. Error bars denote one standard deviation (±) from the mean value ($n \geq 20$). The coarse-textured layer in the layered systems (5b) is demarcated by the two horizontal solid lines. The horizontal dotted line in 5(b) denotes approximately the upper limit of the observed capillary barrier above the coarse layer.

a decreasing rate) with time throughout the experiment. Clearly, the high-temperature, high-wind conditions at the surface expe- dited the subsurface moisture dynamics (Fig. 5). Nonetheless, for a given experiment, the subsurface moisture distribution (and hence presumably the moisture induced effects on methane migration) remained largely unchanged with respect to the selected surface-subsurface controls.

3.1.3. *Depth-wise variation of methane concentration*

Methane concentration profiles in the soils are shown in Fig. 6 for all 24 scenarios studied. Note that the three profiles shown in each subfigure (a through h) correspond to the three wind veloci- ties (0, 0.5, 2.0 ms^{-1}). Evidently, subsurface methane concentration profiles for both the homogeneous and layered systems depicted no distinct effects of wind (when other parameters remained unchanged), suggesting that wind has made no noticeable con- trol on subsurface migration of methane. Importantly, even for the measurements immediately below the surface (i.e., at 0 to 0.5 cm depth) where some wind-induced effects could be expected within a penetrative boundary layer, methane concentrations for different wind speeds were mostly within the range of intrinsic uncertainty (within one SD from the mean as shown by error bars) indicat- ing no clear (or macroscopically distinguishable) effects of wind

on subsurface methane migration. A similar observation was also made by Kimball and Lemon (1971) whose results for mixing hep- tane in fine textured-media under induced surface wind conditions were also affected by the large scatter in measured data. The results corroborate the observations from past studies, for example that of Ishihara et al. (1992) who noted that for fine-textured media of 0.2–0.5 mm size (which resembles the grain size of # 30/40), the mixing depth does not extend beyond a magnitude of 1–10 times grain diameter. They further noted that a considerable mix- ing depth could be observed for high permeable coarse-textured media with a diameter > 10 mm. In fact, both air permeability (k_a, μm^2) and pore size of the medium may control the permissible air penetration depth under a given surface wind condition. Based on a field study, Maier et al. (2012) reported that the ratio of air per- meability to air content (k_a/e) should exceed 1000 μm^2 in order for the turbulence-induced near-surface gas transport (referred to as pressure/barometric pumping) to be statistically significant. For this study, the maximum k_a/e ratio (for dry #30/40 sand) does not exceed approx. 350 μm^2 and hence confirms that wind-induced barometric pumping may not play a significant role in the soil-atmosphere gas exchange process (note that barometric pressure differential within and outside the laboratory was found to be negli- gible). Thus, the overall results suggest that for fine-textured media

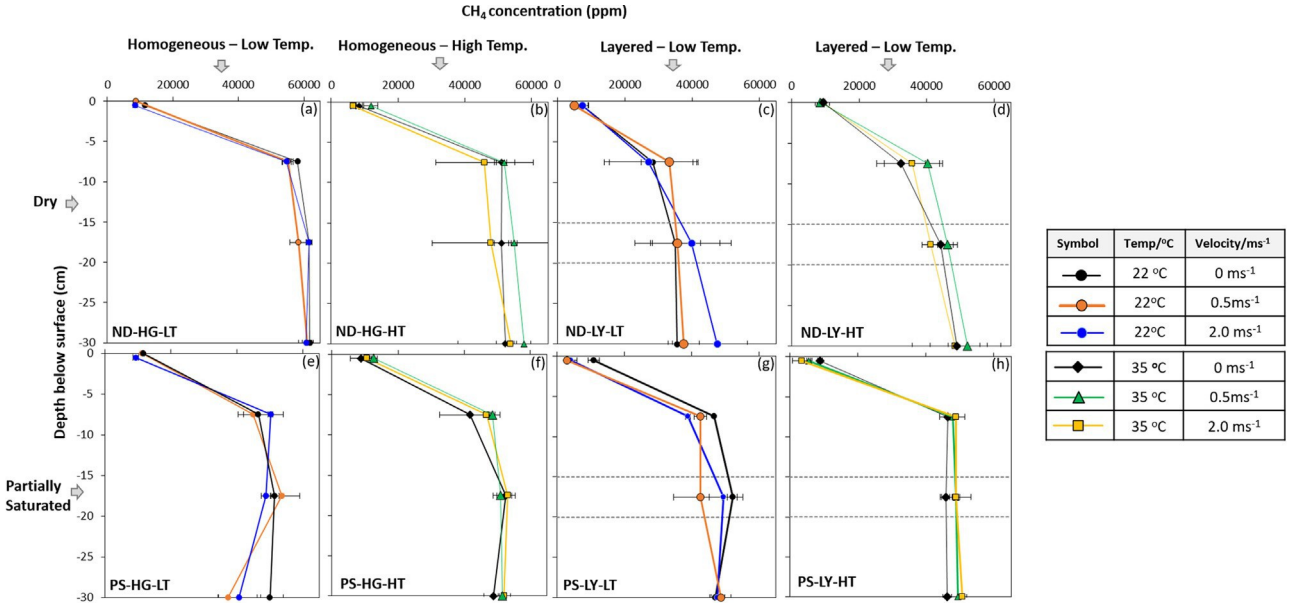

Fig. 6. Observed depth-wise methane concentration profiles for the 24 experimental conditions. Measurements for three wind velocities (0, 0.5, 2.0 ms^{-1}) are shown in corresponding colors in each sub-figure. Error bars denote one standard deviation (±) from the mean value ($n = 3$).

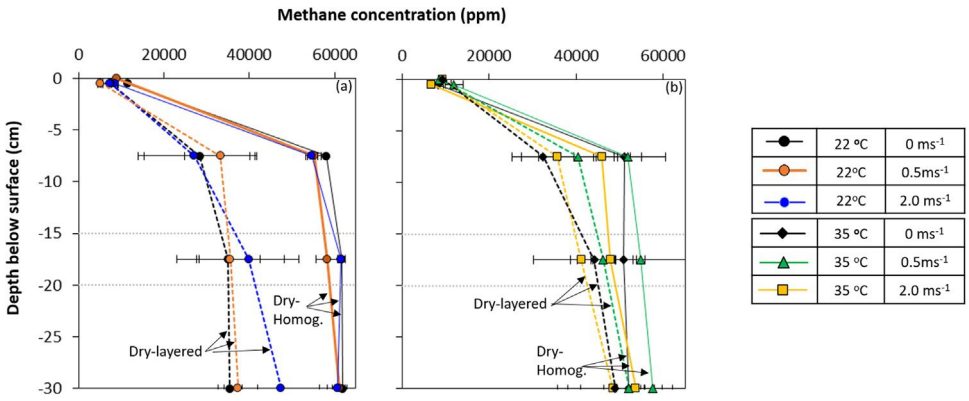

Fig. 7. Observed depth-wise methane concentration profiles for selected homogenous and layered systems for (a) low temperature and (b) high temperature conditions. Error bars denote one standard deviation (±) from the mean value (n = 3). Note that the coarse-textured layer is demarcated by the horizontal lines which are relevant only to the layered systems.

(grain size < 0.5 mm) the gas exchange across the soil-atmosphere interface is predominantly diffusion-controlled which reaffirms the conclusions of Kimball and Lemon (1971).

3.1.4. Effect of textural heterogeneity

The effect of soil layering, was discernable in the CH_4 concen- tration profiles as seen in Fig. 7. For example, the variation of CH_4 concentration with depth for near-dry, layered systems was markedly lower with a steeper concentration gradient than those for near-dry, homogenous systems (Fig. 7a). Similar CH_4 concen- tration profiles in variable permeability soil systems have been observed in past experimental and numerical studies (e.g., Jiránek, 2010). We attribute the relatively low CH_4 concentration in the lay- ered system to improved mixing and migration of CH_4 within the coarse-textured layer compared to the find textured layers. Note that the average pore size in the coarse-textured (# 12/20) sand is almost twice as large as that in the fine-textured (# 30/40) sand and the former (# 12/20) shows four-fold permeability as com- pared to the latter (# 30/40) (see Table 1). This essentially implies the presence of large, well-connected and less tortuous pore space in the coarse-textured (# 12/20) sand in comparison to the fine- textured sand as also noted by Chamindu Deepagoda and Elberling, 2015. Consequently, rapid mixing and migration (both in lateral and vertical directions) of CH_4 within the coarse-textured layer is expected, causing decreased CH_4 concentrations within the layer. Since mixing and migration are higher for the low-density CH_4 compared to the high-density N_2, the gas mixture consisting of CH_4, N_2 and air in the pore space in the underlying fine-textured layer also becomes less CH_4-dominant, causing decreased CH_4 con- centrations in the bottom fine-textured layer as well. Nonetheless, near-surface methane concentrations for both homogenous and layered systems become comparable in order to have balanced inflow (at the point of leakage) and outflow (diffusive emissions off the surface) rates at the steady state (assuming advective flow is not likely a mechanism at the surface as discussed before). We note, however, that the data for the layered systems showed marked variation compared to those for the homogenous systems (shown by the error bars) due to the effects of localized mixing within the coarse layer. For high-temperature conditions (Fig. 7b), however, the effect of layering was not apparent and likely normalized due to the large variability in the measured data.

3.1.5. Effect of saturation

The degree of saturation is a key controller for gas migration in variably saturated porous media since both air permeability and gas diffusivity are strongly moisture-dependent parameters (Sallam et al., 1984; Springer et al., 1998). Previous laboratory-based methane transport studies highlighted the effect of saturation on steady-state methane migration (e.g., changes in the dispersion coefficient; Batterman et al., 1995). Revisiting Fig. 6, the effect of saturation is not immediately visible (within the measurement uncertainty) from the measured subsurface CH_4 concentration data for partially-saturated homogenous systems. A few measurements at partially-saturated conditions (e.g., low-temperature, high-wind conditions; Fig. 6e) showed lower CH_4 concentration at 30 cm depth, but this behavior was not consistent with other data. How- ever, the effect of saturation was apparent in partially-saturated layered systems, especially for the bottom layers (e.g., −10 to 30 cm) where high CH_4 concentrations were observed compared to dry conditions. This is due to the increased water-induced tortu- osity for methane diffusion as will be discussed later. Notably, the presence of the high-saturation layer within the capillary barrier did not cause any appreciable change in the steady-state CH_4 concentration that was discernable from the measured data within the range of uncertainty. Literature presenting the effect of saturation on methane concentration profiles could not be found for direct comparison with our data, hence justifying the need for numerical simulations (below). In fact, the effect of saturation could be better described based on the simulated data as will be discussed later.

3.2. Numerical simulations

Fig. 8 shows the TOUGH2/EOS7CA-simulated methane concen- tration profiles for different subsurface conditions together with the measured data for no-wind conditions. The above-surface wind effects on subsurface methane migration were not accounted for in the numerical simulations since the TOUGH2/EOS7CA code is not formulated to simulate wind-induced surface-atmosphere inter- actions. However, we did account for the effects of temperature (and thereby also the changes in temperature-dependent proper- ties of methane) on subsurface flow and transport of methane. For no-wind conditions, we observed a good agreement between mea- sured and simulated data (note that the simulations involved no fitting or inversely-estimated parameters), showing the promis- ing applicability of the model for simulating subsurface methane migration. The observed good agreement between the measured and simulated data also implies the successful verification of our hypothesis that multiphase migration of multicomponent gas mix- ture (including methane) under density-dependent flow can be adequately represented with a Fickian ADM framework, as also evi- denced

by Okamoto and Gomi (2011). It should, however, be noted that the effect of the presence of a temperature gradient on Fickian diffusion-based multicomponent gas migration is not tested herein since the temperature gradient within the soil is small under the

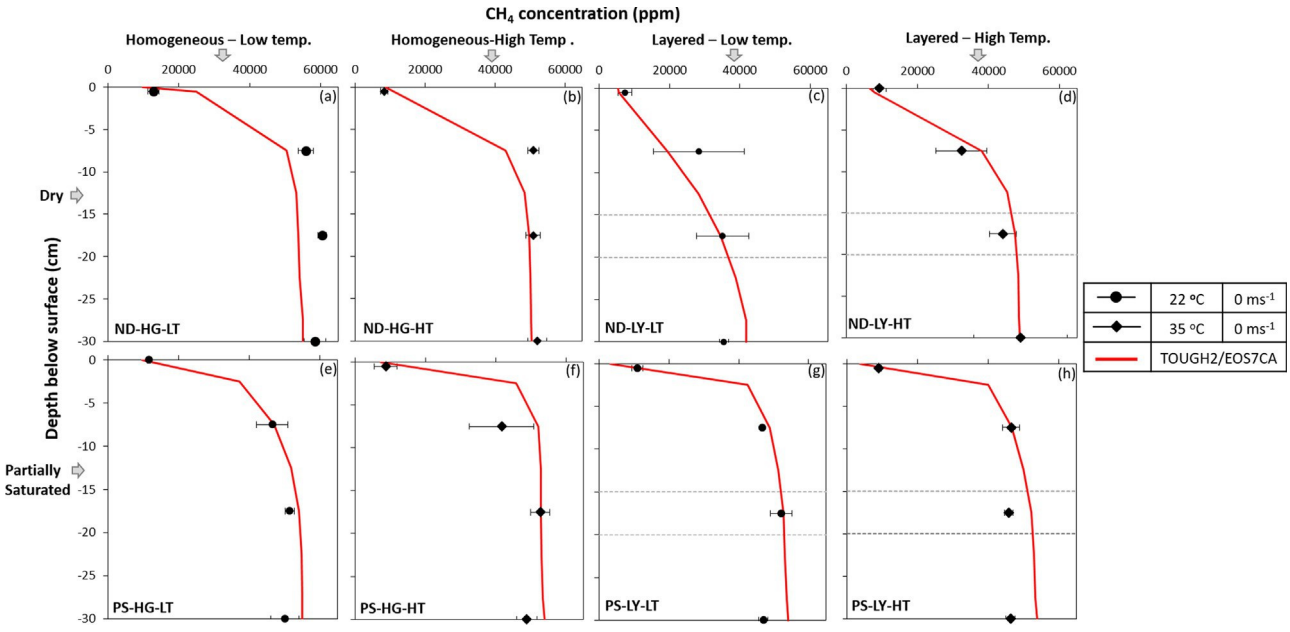

Fig. 8. Measured and TOUGH2/EOS7CA-sumulated methane concentration profiles for no-wind (u = 0 ms^{-1}) conditions. The horizontal dotted line (in 4c, d, g, and h) demarcates the coarse-textured layer in layered systems.

no-wind conditions (see Fig. 4) and the Okamoto and Gomi (2011) study was isothermal. We await further experimental data to test the model applicability for fully-coupled heat and multicomponent gas flow simulations with larger temperature gradients. We further note that no methane oxidation was accounted for within the ADM framework considering high chemical and biological purity of the porous media as discussed previously.

As shown in Fig. 9, the measured and simulated data for satu- ration agreed very well for both (a) homogenous and (b) layered soil systems. Note that in homogenous systems, the data under- estimated by the model (encircled by a solid line in Fig. 9a) correspond to the saturation values in the vicinity of the point of the pipe leakage, implying that gas flow caused water to displace from the soil near the point source pore spaces to more distant pores where the simulated saturation increased over the mea- sured values (encircled by a dotted line in Fig. 9a). This is more clearly illustrated graphically in Fig. 9(b) together with the com- plete saturation profile across the depth. Corresponding profiles for a partially-saturated layered system are shown in Fig. 9(c) and (d), respectively while Fig. 9(d) illustrates the capillary barrier overly- ing the coarse-textured layer (demarcated by the horizontal white lines).

The model-derived steady-state contour maps showing the migration of the gaseous methane plume are shown for four selected scenarios in Fig. 10. Note that due to the low specific grav- ity, methane shows a tendency to preferentially move upward by buoyancy while lateral and downward movements are tortuosity led primarily by diffusion. As a result, methane contours appear as asymmetric and upward-bulging curves (see Fig. 10b–d). At close proximity to the point of leakage, both advective (pressure-driven) and diffusive (concentration-driven) transport occurs, however the flow becomes more and more diffusion-controlled as methane moves away from the source (Okamoto and Gomi, 2011). Since the diffusive methane fronts become nearly horizontal towards the surface and thus become weakly linked to the source, track- ing down the source/leak based on near-surface concentration measurements is challenging in many practical situations, and is further complicated by the different subsurface conditions. In the homogenous system under dry conditions (Fig. 10a), buoyancy-induced upward methane movement is readily supported by the lateral diffusion (due to a high diffusion coefficient at dry con- ditions; Table 1) and therefore the source concentration prevails in the domain at steady state. However, in the layered system under the same conditions (Fig. 10b), both the buoyancy-driven upward movement and the diffusion-driven lateral movement are more pronounced (due to the presence of the high permeability coarse-textured layer), causing the steady-state methane to sta- bilize with a distinct vertical concentration gradient across the system. In the presence of water, methane solubility affects the gaseous phase methane distribution while gaseous methane move- ment is further retarded by limited air-filled pore space (since part of the total pore space is occupied by water), simultaneous movement of water vapor in the gaseous phase, and increased (water-induced) gaseous phase tortuosity and discontinuity. Con- sequently, under partially-saturated conditions, (Fig. 10c and d), the diffusion-controlled lateral movement is more hindered than the buoyancy-induced upward movement of methane as demon- strated by the bulb-shaped distribution profiles. Note that the differences in the two partially-saturated systems (Fig. 10c and d) are not as great as the corresponding profiles for dry condi- tions (Fig. 10a and b), implying the dominant effects of saturation over texture in a predominantly diffusion-controlled gas trans- port system as also observed in many past studies (e.g., Moldrup et al., 2000; Rolston and Moldrup, 2002). In fact, a close obser- vation shows that the methane contours tend to “follow” the saturation profiles illustrating the distinct effects of saturation on subsurface gas migration. Such effects, however, were not clear in measured data due to high variability. The concentration pro- files for high-temperature measurements do not vary significantly from corresponding low-temperature profiles and therefore have not been illustrated here. Additional experimental and numer- ical studies focusing on multiphase flow of methane migration under differently-textured and variably-statured soils are needed to further clarify these effects. Another practically important con- sideration, which was not discussed herein, is methane migration under predominantly advection-controlled conditions (for exam- ple, a gas leakage from a shallow, high-pressure transmission main).

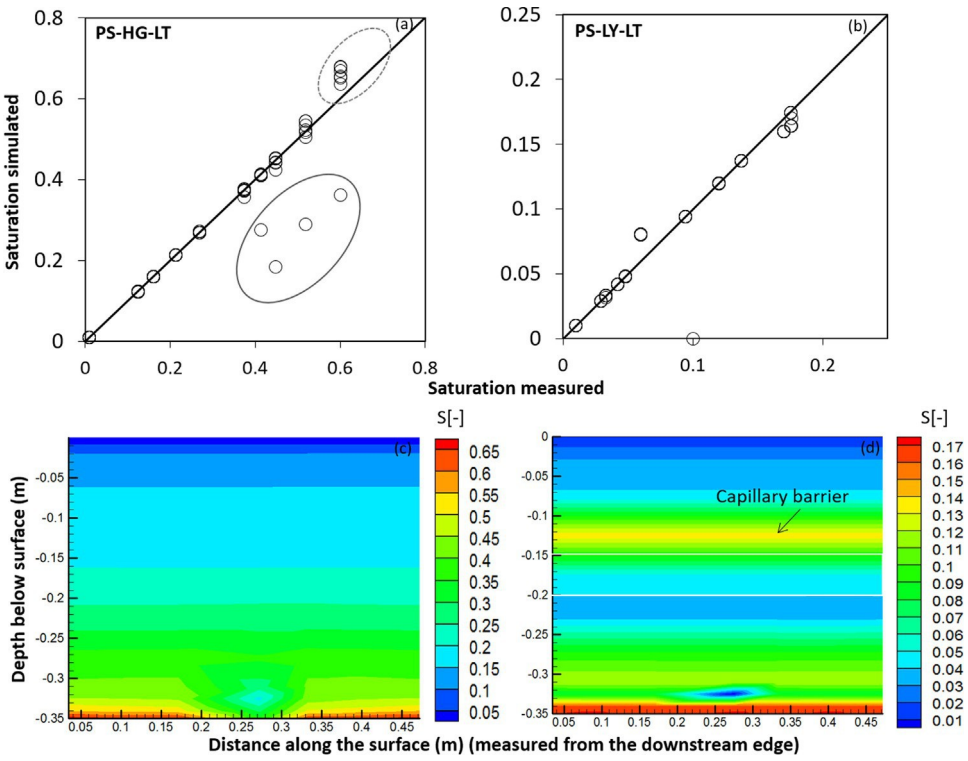

Fig. 9. Scatterplots showing measured and TOUGH2/EOS7CA-simulated saturation for the partially-saturated (a) uniform and (b) layered systems. Error bars denote one standard deviation (±) from the mean value (n = 3). The under-simulated data encircled in solid line correspond to the saturation in the neighborhood of the gas source and while those over-simulated by the model are encircled in dotted lines. The corresponding saturation contours for the two systems are shown graphically in fig. (c) and (d), respectively. The dotted horizontal white lines in (d) demarcate the coarse-textured layer.

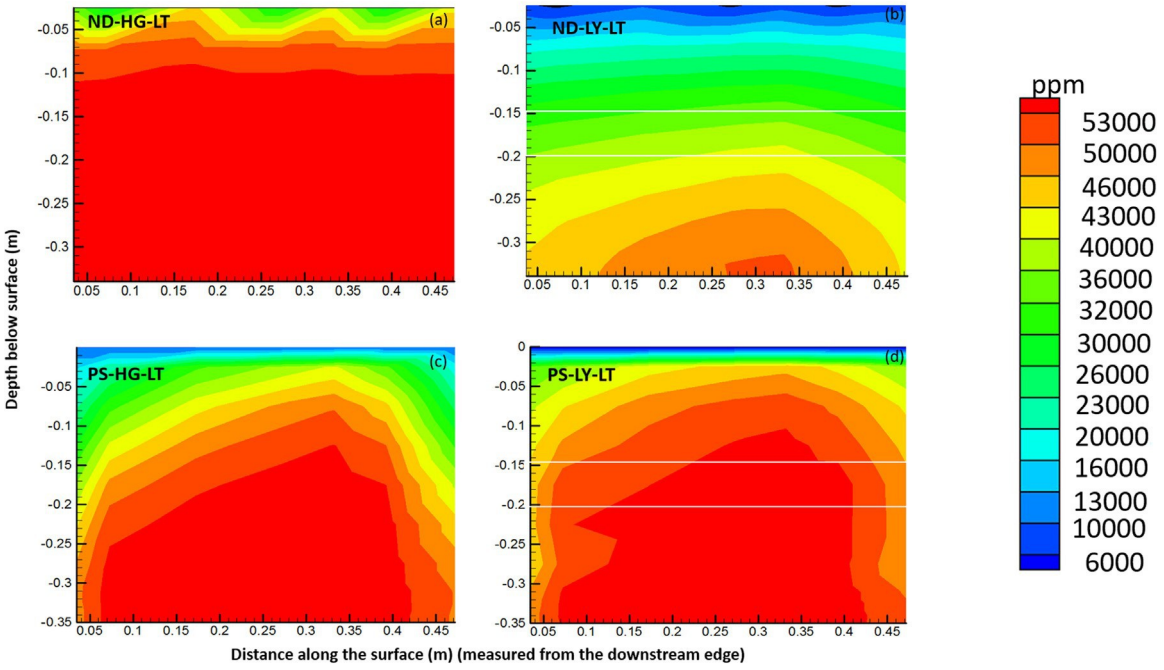

Fig. 10. Concentration maps derived from and TOUGH2/EOS7CA simulations for four selected soil systems. The horizontal white lines (in b and d) demarcate the coarse- textured layer in layered systems.

Finally, we emphasize that the results of the present study are essentially applicable to the selected boundary conditions and length scales in experimental and numerical domains which may not be truly representative of more realistic and practically impor- tant soil-atmosphere continuum scales under field conditions. For

example, the results may significantly vary under barometrically influenced field conditions since pressure induced advective emissions of gases may potentially dominate over diffusion-controlled emissions (Elberling et al., 1997). Also, methane oxidation in microbiologically active field soils may typically range between 4.7 and

16.7 μg CH_4 m^{-2} h^{-1}, depending upon soil type/texture, land use and soil moisture status (Boeckx et al., 1997) and hence could be a key mechanism controlling methane emissions. Therefore, care needs to be taken in generalizing the present results and apply- ing them to (or comparing them with) field-scale conditions where additional complexities may also play important roles at larger scales. The study thus provides valuable experimental and numer- ical insights for future field-scale studies on methane dynamics to further investigate atmospheric and subsurface control mech- anisms and thereby to find appropriate strategies to mitigate methane migration from buried shallow leaky gas infrastructure.

4. Conclusions

Based on a series of controlled laboratory experiments using a two-dimensional bench-scale porous media test facility cou- pled with an open-return wind tunnel, this study investigated the effects of near-surface atmospheric controls (wind and tempera- ture) and soil conditions (textural heterogeneity and soil moisture) on methane transport in the shallow subsurface. Wind velocity showed a more pronounced effect on steady-state surface methane concentration as compared to temperature. The observed decreas- ing surface methane concentration with increasing wind speed could be expressed by a two-parameter nonlinear power function. Temperature effects at no-wind conditions were affected by large variability in measured data while the wind effects obscured the temperature effects at high-wind conditions. Yet, the wind effects were not particularly evident in subsurface methane concentra- tion measurements due likely to limited mixing/penetration depth combined with low permeability in fine-textured porous media.

Clear effects of soil textural heterogeneity and, to a varying degree, of soil moisture were observed in steady-state subsur- face methane concentration profiles. The distinctly low methane concentration across the depth in layered systems was attributed to the rapid mixing and migration of methane within the high-permeability coarse-textured layer. The subsurface methane concentration profiles for no-wind conditions could be adequately simulated using the TOUGH2/EOS7CA simulator based on mul- tiphase, density-dependent flow and transport of methane, air, and water vapor with a Fickian ADM framework. Temperature effects were not pronounced in observed and simulated subsurface methane concentration profiles under no-wind conditions. Some important effects, for example, the dominant effect of saturation over soil texture, could also be inferred from numerical characteri- zation. We emphasize that the experimental and numerical results are essentially valid for the selected length scales of the study and should be extended to larger scale applications with caution.

Acknowledgements

This research was funded in part by the Department of Energy's National Energy Technology Laboratory (NETL), the Research Part- nership to Secure Energy for America project (#RFP2012UN001) and the National Science Foundation Project Award Number 1447533. The research grant from the University of Peradeniya, Sri Lanka (URG/2016/33/E) is also acknowledged. Any opinion, find- ings, and conclusions or recommendations expressed herein are those of the authors and do not necessarily reflect the views of those providing technical input or financial support. The trade names mentioned herein are merely for identification purposes and does not constitute endorsement by any entity involved in this study.

References

American Petroleum Institute and America's Natural Gas Alliance (API/ANGA), 2012. Characterizing Pivotal Sources of Methane Emissions from Natural Gas Production Summary and Analyses of API and ANGA Survey Responses, Final Report, Updated September 2012.

Abriola, L.M., Pinder, G.F., 1985a. A multiphase approach to the modeling of porous-media contamination by organic-compounds. 1. Equation development. Water Resour. Res. 21 (1), 11–18.

Abriola, L.M., Pinder, G.F., 1985b. A multiphase approach to the modeling of porous-media contamination by organic-compounds. 2. Numerical simulations. Water Resour. Res. 21 (1), 19–26.

Basirat, F., Sharma, P., Fagerlund, F., Niemi, A., 2015. Experimental and modeling investigation of CO 2 flow and transport in a coupled domain of porous media and free flow. Int. J. Greenh. Gas Control. 42, 461–470.

Batterman, S., Kulshrestha, A., Cheng, H., 1995. Hydrocarbon vapor transport in low moisture soils. Environ. Sci. Technol. 29 (1), 171–180.

Boeckx, P., Van Cleemput, O., Villaralvo, I., 1997. Methane oxidation in soils with different textures and land use. Nutr. Cycl. Agroecosyst. 49 (91), http://dx.doi.org/10.1023/A:1009706324386.

Brandt, A.R., Heath, G.A., Kort, E.A., O'sullivan, F., Pétron, G., Jordaan, S.M., Tans, P., Wilcox, J., Gopstein, A.M., Arent, D., Wofsy, S., Brown, N.J., Bradley, R., Stucky, G.D., Eardley, D., Harris, R., 2014. Energy and environment methane leaks from North American natural gas systems. Science 343, 733–735.

Cathles, L.M., Brown, L., Taam, M., Hunter, A., 2012. A commentary on The greenhouse gas footprint of natural gas in shale formations by R.W. Howarth, R. Santoro, and Anthony Ingraffea. Clim. Change, http://dx.doi.org/10.1007/ s10584-011-0333-0.

Chamindu Deepagoda, T.K.K., Elberling, B., 2015. Characterization of diffusivity-based oxygen transport in Arctic organic soil. Eur. J. Soil Sci., http:// dx.doi.org/10.1111/ejss.12293.

Chamindu Deepagoda, T.K.K., Smits, K.M., Ramirez, J., Moldrup, P., 2016. Characterization of thermal, hydraulic, and gas diffusion properties in variably saturated sand grades. Vadose Zone J., http://dx.doi.org/10.2136/vzj2015.07. 0097.

Cramer, S.D., 1982. The Solubility of Methane, Carbon Dioxide, and Oxygen in Brines from 0 °C to 300 °C, U.S. Bureau of Mines: Report No. 8706.

Cunningham, R.E., Williams, R.J.J., 1980. Diffusion in Gases and Porous Media (Vol. 1). Plenum Press, New York.

Davarzani, H., Smits, K., Tolene, R.M., Illangasekare, T., 2014. Study of the effect of wind speed on evaporation from soil through integrated modeling of the atmospheric boundary layer and shallow subsurface. Water Resour. Res. 50, 1–20.

Delahaye, C.H., Alonso, E.E., 2002. Soil heterogeneity and preferential paths for gas migration. Eng. Geol. 64 (2), 251–271.

EPA, 2014. Inventory of U.S. GHG Emissions and Sinks: 1990–2012. EPA 430-R-14-003. EPA, Washington, D.C, Accessed October 2016: https://www3. epa.gov/climatechange/test/climatechange/Downloads/ghgemissions/US- GHG-Inventory-2014-Chapter-Upfront.pdf.

Elberling, B., Larsen, F., Christensen, S., Postma, D., 1997. Gas transport in a confined unsaturated zone during atmospheric pressure cycles. Water Resour. Res. 34 (11), 2855–2862.

Folga, S., 2007. Natural Gas Pipeline Technology Overview. Argonne National Laboratory, Argonne Illinois.

GRI/EPA, 1996. In: Harrison, M.R., Shires, T.M., Wessels, J.K., Cowgill, R.M. (Eds.), Emissions from the Natural Gas Industry Vol. 1: Executive Summary; 94/0257. Gas Research Institute/Environmental Protection Agency, Chicago, Accessed October 2016: https://www.epa.gov/sites/production/files/2016-08/ documents/1 executiveummary.pdf.

GTI, 2013. Improving Methane Emission Estimates for Natural Gas Distribution Companies: Phase II-PE Pipes; Report No. 21044; OTD Project Number 7.10.c. Gas Technology Institute, Des Plaines, IL2013.

Hibi, Y., Fujinawa, K., Nishizaki, S., Okamura, K., Tasaki, M., 2009. Multi-component migration in the gas phase of soil: comparison between results of experiments and simulation by dusty gas model. Soils Found. 49, 569–581.

Hibi, Y., Kanou, Y., Ohira, Y., 2012. Estimation of mechanical dispersion and dispersivity in a soil-gas system by column experiments and the dusty gas model. J. Contam. Hydrol. 131 (1), 39–53.

Ho, C.K., Webb, S.W. (Eds.), 2006. Gas Transport in Porous Media. Springer.

Howarth, R.W., Santoro, R., Ingraffea, A., 2011. Methane and the greenhouse-gas footprint of natural gas from shale formations. Clim. Change 106, 679–690.

Intergovernmental Panel on Climate Change (IPCC), 2011. In: Edenhofer, O.,

Pichs-Madruga, R., Sokona, Y., Seyboth, K., Matschoss, P., Kadner, S., Zwickel, T., Eickemeier, P., Hansen, G., Schlomer, S., von Stechow, C. (Eds.), IPCC Special Report on Renewable Energy Sources and Climate Change Mitigation. Prepared by Working Group III of the Intergovernmental Panel on Climate Change. Cambridge University Press, Cambridge, United Kingdom and New York, NY, USA, 1075 pp.

Intergovernmental Panel on Climate Change (IPCC), 2014. Mitigation of Climate Change: Energy Systems. Fifth Assessment Report. Cambridge University Press, Cambridge, U.K.

Ishihara, Y., Shimojima, E., Harada, H., 1992. Water vapor transfer beneath bare soil where evaporation is influenced by a turbulent surface wind. J. Hydrol. 131, 63–104.

Jackson, R.B., Down, A., Phillips, N.G., Ackley, R.C., Cook, C.W., Plata, D.L., Zhao, K., 2013. Natural gas pipeline leaks across Washington, DC. Environ. Sci. Technol. 48, 2051–2058.

Jiránek, M., 2010. Application on of numerical modelling for the better design of radon preventive and remedial measures. Nukleonika 55, 451–457, ISSN 0029-5922.

Karion, A., Sweeney, C., Pétron, G., Frost, G., Michael Hardesty, R., Kofler, J., Miller, B.R., Newberger, T., Wolter, S., Banta, R., Brewer, A., Dlugokencky, E., Lang, P., Montzka, S.A., Schnell, R., Tans, P., Trainer, M., Zamora, R., Conley, S., 2013. Methane emissions estimate from airborne measurements over a western United States natural gas field. Geophys. Res. Lett. 40, 4393–4397.

Karl-Heinz, A.A., Wolf, N.S., Bruining, J., 2004. Multiphase flow experiments in order to understand the behavior of (partly) saturated coals as a gas reservoir: examples. Geol. Belgica 7, 15–121.

Kimball, B.A., Lemon, E.R., 1971. Air turbulence effects upon soil gas exchange. Soil Sci. Soc. Am. J. 35, 16–21.

Lamb, B.K., Edburg, S.L., Ferrara, T.W., Howard, T., Harrison, M.R., Kolb, C.E., Townsend-Small, A., Dyck, W., Possolo, A., Whetstone, J.R., 2015. Direct measurements show decreasing methane emissions from natural gas local distribution systems in the United States. Environ. Sci. Tech. 49 (8), 5161–5169.

Lelieveld, J., Lechtenböhmer, S., Assonov, S.S., Brenninkmeijer, C.A.M., Dienst, C., Fischedick, M., Hanke, T., 2005. Greenhouse gases: low methane leakage from gas pipelines. Nature 434, 841–842.

Levi, M.A., 2012. Comment on hydrocarbon emissions characterization in the Colorado Front Range: a pilot study by Gabrielle Pétron et al. J. Geophys. Res. D: Atmos. 117.

Levi, M., 2013. Climate changes of natural gas as a bridge fuel. Clim. Change 118, 609–623.

Maier, M., Schack-Kirchner, H., Aubinet, M., Goffi, S., Longdoz, B., Parent, F., 2012. Turbulence effect on gas transport in three contrasting forest soils. Soil Sci. Soc. Am. J. 76, 1518–1528, http://dx.doi.org/10.2136/sssaj2011.0376.

Mason, E.A., Malinauskas, A.P., 1983. Gas Transport in Porous Media: the Dusty-Gas Model (Vol. 17). Elsevier Science Ltd.

Moldrup, P., Olesen, T., Gamst, J., Schjønning Yamaguchi, T., Rolston, D.E., 2000. Predicting the gas diffusion coefficient in repacked soil: water induced linear reduction model. Soil Sci. Soc. Am. J. 64, 1588–1594.

Okamoto, H., Gomi, Y., 2011. Empirical research on diffusion behavior of leaked gas in the ground. J. Loss Prev. Process Ind. 24, 531–540.

Okamoto, H., Gomi, Y., Akagi, H., 2014. Movement characteristics of hydrogen gas within the ground and its detection at ground surface. J. Civil Eng. Sci. 3, 49–66.

Oldenburg, C.M., Unger, A.J.A., 2004. Coupled vadose zone and atmospheric surface layer transport of carbon dioxide from geologic carbon sequestration sites. Vadose Zone J. 3, 848–857.

Oldenburg, C.M., Webb, S.W., Pruess, K., Moridis, G.J., 2004. Mixing of stably stratified gases in subsurface reservoirs: a comparison of diffusion models. Transp. Porous Media 54 (3), 323–334.

Oldenburg, C.M., 2015. EOS7CA Version 1.0: TOUGH2 Module for Gas Migration in Shallow Subsurface Porous Media Systems, Lawrence Berkeley National Laboratory Report LBNL-175204.

Pétron, G., Frost, G., Miller, B.R., Hirsch, A.I., Montzka, S.A., Karion, A., Trainer, M., Sweeney, C., Andrews, A.E., Miller, L., Kofler, J., Bar-Ilan, A., Dlugokencky, E.J., Patrick, L., Moore, C.T., Ryerson, T.B., Siso, C., Kolodzey, W., Lang, P.M., Conway, T., Novelli, P., Masarie, K., Hall, B., Guenther, D., Kitzis, D., Miller, J., Welsh, D., Wolfe, D., Neff, W., Tans, P., 2012. Hydrocarbon emissions characterization in the Colorado Front Range: a pilot study. J. Geophys. Res. 117, D04304.

Peng, D.Y., Robinson, D.B., 1976. Ind. Eng. Chem. Fundam. 15, 59–64. Phillips, N.G., Ackley, R., Crosson, E.R., Down, A., Hutyra, L.R., Brondfield, M., Jonathan, D.K., Zhao, K., Jackson, R.B., 2013. Mapping urban pipeline leaks: methane leaks across Boston. Environ. Pollut. 173, 1–4.

Poulsen, T.G., Moldrup, P., Christophersen, M., Kjeldsen, P., 2003. Relating landfill gas emissions to atmospheric pressure using numerical modelling and state-space analysis. Waste Manage. Res. 21, 356–366.

Pruess, K., Oldenburg, C.M., Moridis, G.J., 1999. TOUGH2 User's Guide Version 2. E.O. Lawrence Berkeley National Laboratory Report LBNL-43134.

Rolston, D.E., Moldrup, P., 2002. Gas diffusivity. In: Dane, J.H., Topp, G.C. (Eds.), Methods of Soil Analysis. Part 4. SSSA Book Ser. 5. ASA and SSSA, Madison, pp. 1113–1139.

Sakaki, T., Limsuwat, A., Smits, K.M., Illangasekare, T.H., 2008. Empirical twopoint a-mixing model for calibrating the ECH2O EC-5 soil moisture sensor in sands. Water Resour. Res. 44, W00D08, http://dx.doi.org/10.1029/2008WR006870.

Sallam, A., Jury, W.A., Letey, J., 1984. Measurement of the gas diffusion coefficient under relatively low air-filled porosity. Soil Sci. Soc. Am. J. 48, 3–6.

Schroth, M.H., Ahearn, S.J., Selker, J.S., Istok, J.D., 1996. Characterization of miller-similiar silica sands for laboratory hydrologic studies. Soil Sci. Soc. Am. J. 60, 1331–1339.

Slough, K.J., Sudicky, E.A., Forsyth, P.A., 1999. Numerical simulation of multiphase flow and phase partitioning in discretely fractured geologic media. J. Contam. Hydrol. 40 (2), 107–136.

Smith, K.A., Ball, T., Conen, F., Dobbie, K.E., Massheder, J., Rey, A., 2003. Exchange of greenhouse gases between soil and atmosphere: interactions of soil physical factors and biological processes. Eur. J. Soil Sci. 54 (4), 779–791.

Smits, K.M., Sakaki, T., Howington, S.E., Peters, J.F., Illangasekare, T.H., 2012. Temperature dependence of thermal properties of sands across a wide range of temperatures (30–70 °C). Vadose Zone J., http://dx.doi.org/10.2136/vzj2012.0033.

Springer, D.S., Loaiciga, H.A., Cullen, S.J., Everett, L.G., 1998. Air permeability of porous materials under controlled laboratory condition. Ground Water 36 (4), 558–565.

Stormont, J., Anderson, C., 1999. Capillary barrier effect from underlying coarser layer. J. Geotech. Geoenviron. Eng. ASCE 125 (8), 641–648.

Taylor, S.A., 1949. Oxygen diffusion in porous media as a measure of soil aeration. Soil Sci. Soc. Am. Proc. 14, 55–61.

Transportation of Natural and Other Gas by Pipeline: Minimum Federal Safety Standards, 49C.F.R. 192.327 2004, 2016. [Online]. Available: http://www.ecfr. gov/cgi-in/retrieveECFR?gp=1&SID=c3b0e911814b61c0f807c43f51ac7bc6 &ty=HTML&h=L&mc=true&r=SECTION&n=se49.3.192 1327 (accessed 22.06.16.).

US Environmental Protection Agency (USEPA), 2003. Lessons Learned: Reducing Methane Emissions from Compressor Rod Packing Systems, Publication Number EPA430-B-03-011, May 2003.

US Environmental Protection Agency (USEPA) Office of Inspector General, 2014. Improvements Needed in EPA Efforts to Address Methane Emissions From Natural Gas Distribution Pipelines, Report No. 14-P-0324, Available at www.epa.gov/oig/reports/2014/20140729-14-P-0325.pdf.

van Genuchten, M.Th., 1980. A closed-form equation for predicting the hydraulic conductivity of unsaturated soils. Soil Sci. Soc. Am. J. 44, 892–898.

Veranth, J.M., Pardyjak, E.R., Seshadri, G., 2003. Vehicle-generated fugitive dust transport: analytic models and field study. Atmos. Environ. 16 (2003), 2295–2303.

Volckaert, G., Ortiz, L., De Cannière, P., Put, M., Horseman, S.T., Harrington, J.F., Fioravante, V., Impey, M.D., 1995. MEGAS: Modelling and Experiments on Gas Migration in Repository Host Rocks CEC. Final Report—Phase 1, Eur 16235-EN.

Webb, S.W., 1996. Gas-Phase Diffusion in Porous Media – Evaluation of an Advective-dispersive Formulation and the Dusty-Gas Model Including Comparison to Data for Binary Mixtures, SAND96-1197. Sandia National Laboratories.

Webb, S.W., 1998. Gas diffusion in porous media – evaluation of an advective-dispersive formulation and the dusty-gas model for binary mixtures. J. Porous Media 1, 187–199.

Yan, Y., Dong, X., Li, J., 2015. Experimental study of methane diffusion in soil for an underground gas pipe leak. J. Nat. Gas Sci. Eng. 27, 82–89.

Table 1
Physical properties and transport parameters of the two porous media.

Porous media #	Particle diameter (D_{50})	Particle density (ρ_d)	Total porosity (Φ)	Bulk density (ρ_b)	Saturated hydraulic conductivity (K_{sat})	Thermal conductivity (λ)		Gas Diffusivity[a] Ds/Do	Van Genuchten parameters[b]			Permeability
	mm	g cm^{-3}	cm^3 cm^{-3}	g cm^{-3}	cm s^{-1}	W m^{-1} K^{-1}			θ_r (cm3 cm−3)	α (cm^{-1})	n (−)	k[c] (m^2)
						λ_{dry}	λ_{sat}	$D_s/D_o\|_{dry}$				
12/20	1.04	2.665	0.33	1.82	0.376	0.314	2.948	0.201	0.056	0.053	13.5	3.8×10^{-10}
30/40	0.53	2.665	0.336	1.77	0.106	0.287	2.887	0.184	0.017	0.1	9.21	1.0×10^{-10}

[a] Measured independently using one-chamber diffusion apparatus (Taylor, 1949), see Chamindu Deepagoda et al. (2016).
[b] $m = 1 - 1/n$.
[c] Estimated from K_{sat} assuming fluidity of 9.81×10^6 m^{-1} s^{-1} at 20 °C.

Table 2
Experimental schedule and the notations used to describe different experimental conditions.

			Above Ground Controls					
			Low Temp. (20–24 °C)			High Temp. (35–38 °C)		
			u = 0 ms^{-1}	u = 0.5 ms^{-1}	u = 2.0 ms^{-1}	u = 0 ms^{-1}	u = 0.5 ms^{-1}	u = 2.0 ms^{-1}
Below Ground Controls	Near dry	Homogeneous	ND-HG-LT			ND-HG-HT		
		Layered	ND-LY-LT			ND-LY-HT		
	Partially-sat	Homogenous	PS-HG-LT			PS-HG-HT		
		Layered	PS-LY-LT			PS-LY-HT		

ND, Near-dry; PS, Partially-saturated; HG, Homogenous; LY, Layered; LT, Low temperature; HT, High temperature

the subsurface migration of methane gas. Three experiments were duplicated (not shown in Table 2) to confirm the repeatability of the measurements. In the following text, we follow the notations in Table 2 (presenting saturation-soil state-temperature combinations) to describe results relevant to the different scenarios.

All the experiments were conducted within a barometrically closed building under invariant barometric pressure conditions. The experimental set up was located within the laboratory in such a way that the induced pressure gradients (e.g, due to opening/closing of doors) minimally influenced the experimental results. The passersby were restricted within the experimental area during the experiments to avoid likely pressure fluctuations. Pressure sensors installed within the building were randomly checked to ensure constant pressure conditions.

2.2. Numerical model

Numerical simulations were performed using the multiphase transport simulator TOUGH2 (Pruess et al., 1999) combined with the equation of state module EOS7CA (Oldenburg, 2015). TOUGH2/EOS7CA simulates the subsurface flow and transport of

Table 3
Governing equations pertinent to this study as solved in TOUGH2/EOS7CA.

Description	Equation
Mass and energy balance	$\frac{d}{dt}\int_V M^\kappa V_n = \int_V \boldsymbol{F}^\kappa . n d\Gamma_n + \boldsymbol{q}^\kappa dV_n$
Mass accumulation	$M^\kappa = \phi \ \Sigma_\beta S_\beta \rho_\beta X^k_\beta$
Phase flux	$\boldsymbol{F}_\beta = -\boldsymbol{k}\frac{k_{r\beta}\rho_\beta}{\mu_\beta}\left(\nabla P_\beta - \rho_\beta g\right)$
Component flux: advective and diffusive	$\boldsymbol{F}^\kappa_{adv} = \sum_\beta X^k_\beta \boldsymbol{F}_\beta$
	$\boldsymbol{F}^\kappa_{dif} = -\phi\tau\rho_\beta D^k_\beta \nabla X^k_\beta;\ D^k_\beta(T) = D^k_\beta(T_o)\left[\frac{T+273.15}{273.15}\right]T_D$
Relative permeability (van Genuchten, 1980)	$\text{if } S_l < S_{ls} k_{rl} = \sqrt{S^*}\left\{1 - \left(1 - [S^*]^{1/\lambda}\right)^\lambda\right\}^2$
	$\text{if } S_l \geq S_{ls} k_{rl} = 1 \quad \text{if } S_{gr} = 0 k_{rg} = 1 - k_{rl}$
	$\text{if } S_{gr} > 0 k_{rg} = \left(1 - \hat{S}\right)^2\left(1 - \hat{S}^2\right)$
	$\hat{S} = (S_l - S_{lr})/(S_{ls} - S_{lr})$
Capillary pressure (van Genuchten, 1980)	$Pc = Po\left([S^*]^{-1/\lambda} - 1\right)^{1-\lambda}$
	subject to $-P_{max} \leq Pc \leq 0$
Henry's law	$P^\kappa_g = K_H X_w$